

Thermally assisted interlayer magnetic coupling through $\text{Ba}_{0.05}\text{Sr}_{0.95}\text{TiO}_3$ barriers

Santiago J. Carreira, Luis Avilés Félix, Martín Sirena, Gabriela Alejandro, and Laura B. Steren

Citation: *Applied Physics Letters* **109**, 062402 (2016); doi: 10.1063/1.4960639

View online: <http://dx.doi.org/10.1063/1.4960639>

View Table of Contents: <http://scitation.aip.org/content/aip/journal/apl/109/6?ver=pdfcov>

Published by the [AIP Publishing](#)

Articles you may be interested in

[Magnetic proximity effect in \$\text{Pr}_{0.5}\text{Ca}_{0.5}\text{MnO}_3/\text{La}_{0.7}\text{Sr}_{0.3}\text{MnO}_3\$ bilayered films](#)

Low Temp. Phys. **38**, 41 (2012); 10.1063/1.3677235

[Magnetization studies in \$\text{IrMn}/\text{Co}/\text{Ru}/\text{NiFe}\$ spin valves with weak interlayer coupling](#)

J. Appl. Phys. **106**, 113903 (2009); 10.1063/1.3257113

[Ferroelectric and structural properties of \$\text{Ba}_{2-x}\text{Sr}_x\text{Nb}_5\text{O}_{15}\$ thin films prepared on \$\text{La}_{0.05}\text{Sr}_{0.95}\text{TiO}_3\$ substrates](#)

J. Appl. Phys. **103**, 084108 (2008); 10.1063/1.2903072

[Oscillatory exchange coupling in \$\text{La}_{0.67}\text{Sr}_{0.33}\text{MnO}_3/\text{SrTiO}_3\$ superlattices](#)

Appl. Phys. Lett. **91**, 012505 (2007); 10.1063/1.2753707

[Ru-doped \$\text{La}_{0.6}\text{Sr}_{0.4}\text{MnO}_3\$ thin films as a coercivity tunable electrode for magnetic tunnel junctions](#)

Appl. Phys. Lett. **86**, 192505 (2005); 10.1063/1.1923199

The advertisement features a blue background with a molecular structure of spheres. On the left is a thumbnail of an 'Applied Physics Reviews' journal cover showing a layered material structure. The main text reads 'NEW Special Topic Sections' in large white font. Below this, it says 'NOW ONLINE' in yellow, followed by 'Lithium Niobate Properties and Applications: Reviews of Emerging Trends' in white. The AIP Applied Physics Reviews logo is in the bottom right corner.

NEW Special Topic Sections

NOW ONLINE
Lithium Niobate Properties and Applications:
Reviews of Emerging Trends

AIP Applied Physics Reviews

Thermally assisted interlayer magnetic coupling through $\text{Ba}_{0.05}\text{Sr}_{0.95}\text{TiO}_3$ barriers

Santiago J. Carreira,^{1,2} Luis Avilés Félix,^{2,3} Martín Sirena,^{2,3,4} Gabriela Alejandro,^{2,3} and Laura B. Steren^{1,2}

¹Centro Atómico Constituyentes, San Martín, Buenos Aires 1650, Argentina

²Consejo Nacional de Investigaciones Científicas y Técnicas, Ciudad Autónoma de Buenos Aires C1425FQB, Argentina

³Centro Atómico Bariloche, Bariloche, Rio Negro 8400, Argentina

⁴Instituto Balseiro-CNEA & Univ. Nac. de Cuyo, Bariloche, Rio Negro 8400, Argentina

(Received 25 April 2016; accepted 27 July 2016; published online 9 August 2016)

We report on the interlayer exchange coupling across insulating barriers observed on $\text{Ni}_{80}\text{Fe}_{20}/\text{Ba}_{0.05}\text{Sr}_{0.95}\text{TiO}_3/\text{La}_{0.66}\text{Sr}_{0.33}\text{MnO}_3$ (Py/BST_{0.05}/LSMO) trilayers. The coupling mechanism has been analyzed in terms of the barrier thickness, samples' substrate, and temperature. We examined the effect of MgO (MGO) and SrTiO₃ (STO) (001) single-crystalline substrates on the magnetic coupling and also on the magnetic anisotropies of the samples in order to get a deeper understanding of the magnetism of the structures. We measured a weak coupling mediated by spin-dependent tunneling phenomena whose sign and strength depend on barrier thickness and substrate. An antiferromagnetic (AF) exchange prevails for most of the samples and smoothly increases with the barrier thicknesses as a consequence of the screening effects of the BST_{0.05}. The coupling monotonically increases with temperature in all the samples and this behavior is attributed to thermally assisted mechanisms. The magnetic anisotropy of both magnetic components has a cubic symmetry that in the case of permalloy is added to a small uniaxial component. *Published by AIP Publishing.*

[<http://dx.doi.org/10.1063/1.4960639>]

In recent years, researchers have renewed their interest in the fundamental physics inherent to the spin dependent tunneling phenomena, which governs the performance of magnetic tunnel junctions.¹ Perovskite manganites and titanates have shown an outstanding potential for spintronics devices, as they show a rich variety of transport and magnetic properties.² In particular, $\text{La}_{0.67}\text{Sr}_{0.33}\text{MnO}_3$ (LSMO) has been extensively studied as a possible source of spin-polarized electrons at room temperature.³ The choice of the tunneling barrier is also a relevant issue to improve the performance of these devices.⁴ Low-doped barium strontium titanate, $\text{Ba}_x\text{Sr}_{1-x}\text{TiO}_3$ (BST_x), has emerged as a good candidate for application in tunable microwave devices due to its large permittivity and high breakdown-field.⁵ These materials present a ferroelectric phase transition at low temperatures and are usually operated above the Curie temperature due to their large permittivity. For instance, the Curie temperature of BST_{0.05} single crystals is around 60 K.⁶

LSMO and BST_{0.05} are distorted perovskites with a pseudo-cubic lattice parameter of 0.387 nm and 0.391 nm, respectively.^{7,8} The small lattice mismatch between both compounds, $\eta = (a_{\text{LSMO}} - a_{\text{BST}_{0.05}})/a_{\text{LSMO}} \sim 1\%$, together with the ferroelectric and insulating character of the BST_{0.05} motivated us to integrate them in a multiferroic tunnel junction.⁹ An asymmetric junction was so designed, integrating as the second electrode a layer of permalloy (Py). This choice has been done taking into account that high-quality Py films can be grown onto oxide substrates in spite of the large lattice mismatch at Py/OX interfaces and its soft magnetic properties.¹⁰ The characteristics of ferromagnetic (FM)/barrier interfaces,¹¹ i.e., creation of ultrathin magnetic layers by charge transfer¹² and/or the existence of magnetic “dead” layers¹³ at them, are known

to play a crucial role in the tunneling magneto-resistance effect. Oxide-based interfaces are particularly reactive and the exchange-bias effect is usually observed in these systems arisen from the appearance of antiferromagnetic layers at the interface of magnetic/non-magnetic layers.¹⁴ The existence of an interlayer exchange coupling (IEC) across ferroelectric barriers has been theoretically predicted by Zhuravlev and coworkers in a recent article.¹⁵ The IEC between ferromagnetic electrodes through an insulating spacer, as shown by Slonczewski,¹⁶ is determined by the evanescent states in the barrier. The coupling, therefore, exhibits a characteristic temperature and thickness dependence.

Here, we study the nature of the magnetic coupling across a ferroelectric barrier in a multiferroic tunnel structure, exploring the effect of substrate and temperature on it. The influence of strains arisen at the substrate/electrode and barrier/electrode interfaces on the magnetic properties of the FM electrodes is also analyzed.

$\text{Ni}_{80}\text{Fe}_{20}/\text{Ba}_{0.05}\text{Sr}_{0.95}\text{TiO}_3/\text{La}_{0.66}\text{Sr}_{0.33}\text{MnO}_3/\text{S}$ trilayers were deposited on single-crystalline substrates (S) by dc magnetron sputtering as described elsewhere.¹⁷ Two series of samples were used in this study with barrier thicknesses t_b , $0.8 \text{ nm} \leq t_b \leq 3.8 \text{ nm}$. One of them, t_b -SrTiO₃ (STO), was grown on (001) STO and the second one, t_b -MgO (MGO), was deposited on MGO. The thickness of LSMO and Py electrodes is 75 nm and 50 nm, respectively, across the whole series of samples. The crystalline structure of the samples was explored by XRD experiments and the surface of the samples was characterized by atomic force microscopy (AFM) and conductive-AFM (C-AFM).¹⁷

These measurements showed that the samples' roughness increases from 0.2 to 0.4 nm as the thickness of the barrier layer

increases from 0.4 nm to 15.2 nm. C-AFM measurements confirm the smooth growth of the barrier layer over the manganite layer, with a good coverage of the ferromagnetic (FM) electrode for barriers' thickness larger than 1.5 nm grown on (001) STO substrates. These results give us valuable information for the analysis of magnetic coupling mechanisms in our samples.

Magnetic measurements were done in a Vibrating Sample Magnetometer (VSM) and 7 T-SQUID magnetometers, with the magnetic field applied along the (100) axis in the plane of the films. Magnetization loops were measured at temperatures between 5 K and 300 K. The measurements in the SQUID were performed in non-overshoot mode and high resolution field option, whereas the VSM measurements were performed in linear mode. In all the cases, the field step was not larger than 1 Oe or 2 Oe and the ramp velocity 0.2 Oe/s maximum. This method was accurate enough to resolve shifts of the hysteresis loops up to 2 Oe. Ferromagnetic Resonance (FMR) measurements were carried out in a commercial Bruker ESP 300 spectrometer. A frequency of 9.5 GHz (X-Band) was used to measure the in-plane angular variation of the resonance field at temperatures between 100 K and 300 K in order to get an insight into the magnetic anisotropy of the samples. The whole set of FMR spectra was collected by rotating the sample while keeping the external magnetic field H always parallel to the sample plane.

The quality of the samples in terms of crystalline structure was investigated by XRD experiments (Figure 1). The lattice mismatch between LSMO and STO is $\sim 1\%$ so the manganite is expected to be weakly tensile strained in the plane of the films. The lattice mismatch is 8% for LSMO/MGO. In these cases, LSMO films are relaxed by misfit dislocations. In both series of samples, LSMO is textured with (00n) parallel to the samples' normal. The Py reflections are much difficult to identify due to their weak signals and their superposition with other peaks in the MGO series of samples. From the analysis in the range $20^\circ < 2\theta < 100^\circ$ of the XRD spectra, the orientations (001) and (110) were identified in samples grown onto MGO substrates (Figure 1(a)) whereas only reflections corresponding to Py (110) and (111) were hardly observed for STO samples (Fig. 1(b)). In general, Py overcomes the large mismatch between the lattice parameters of films and oxides by creating dislocations.^{18–20} Under these circumstances, FMR

becomes a suitable tool to characterize the symmetry of the magnetic anisotropy of the system, and so to infer some information about its orientations as will be discussed below.

FMR spectra show, at $T = 250$ K, two resonance lines associated with the Py and the LSMO layers, respectively, separated by a 2 nm $\text{BST}_{0.05}$ spacer. (Figure 2(a)) The measuring temperature was chosen in order to have the two magnetic components well resolved, while both Py and LSMO are still in the ferromagnetic phase. Fig. 2(b) plots the in-plane angular variations of the resonance field of permalloy, namely, $H_{\text{res-Py}}$. Note that the overall magnetic anisotropy of the Py layer is very small. It is well described by a four-fold cubic symmetry of the magnetocrystalline term with $K_4 \approx 3 \times 10^3 \text{ erg/cm}^3$, superimposed with a tiny uniaxial component. The FMR results are consistent with the XRD ones that reveal the presence of different orientations of Py in the multilayers and agree with previous references.^{10,21} The LSMO layer also shows a cubic magnetic anisotropy²² as expected from the pseudo-cubic structure of the compound with $K_4 \approx 1.5 \times 10^4 \text{ erg/cm}^3$ at 250 K.

A typical magnetization loop is shown in Fig. 3(a). It can be noticed that the magnetization reversal occurs in two-steps, suggesting that the Py and LSMO are weakly coupled or not coupled at all. A notable difference of Py and LSMO coercive fields, softer and harder contributions, respectively, is reflected on the loops. A magnetization plateau is noticed at intermediate fields where an antiparallel arrangement (AP) of both magnetizations is set.

The magnetization loops are strongly affected by substrates and barrier thickness. In order to get a first characterization of the magnetization reversal of both components, the coercive fields of the LSMO and Py layers were calculated by averaging the coercive fields at the inflexion point for increasing (H_c^+) and decreasing (H_c^-) magnetic field loops' branches. The curves were differentiated numerically and the corresponding peaks were fitted with a Gaussian function to finally determine the coercive field as the mean value of the fit. In Figs. 3(b) and 3(c), we show the variation of the Py and LSMO coercive fields with the spacer thickness and different substrates. As outlined above, both coercive fields are

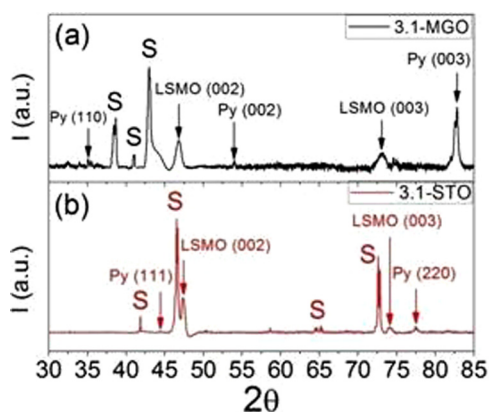


FIG. 1. XRD patterns of $t_b = 3.1$ nm for (a) MGO and (b) STO substrates.

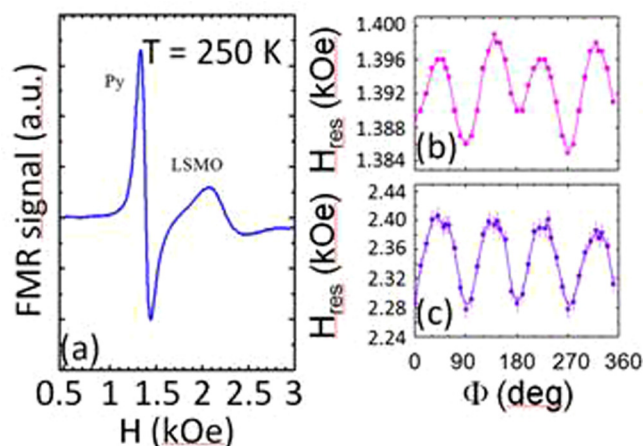


FIG. 2. (a) FMR spectrum of a 0.8-MGO trilayer, recorded at $T = 250$ K in the in-plane experimental set-up. (b) In-plane angular variation of the resonance field (H_{res}) of (top) Py and (bottom) LSMO layers.

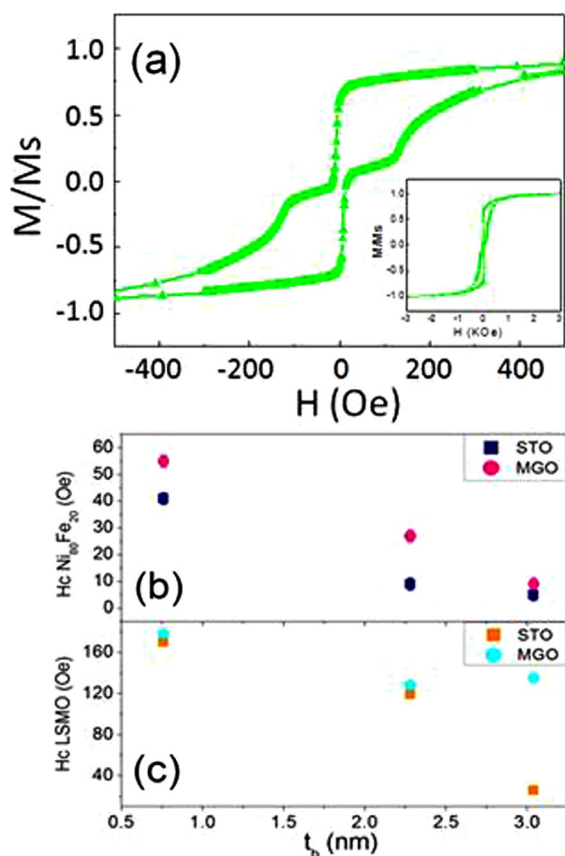


FIG. 3. (a) Hysteresis loop of a 3.1-MGO trilayer, measured at 51 K with the field oriented parallel to the 100 crystallographic direction of the substrate. Inset: Full hysteresis cycle taken between 1 T and -1 T. Coercive field vs. spacer thickness for (b) Py and (c) LSMO layers. (■) and (●) symbols correspond to samples deposited on STO and MGO substrates, respectively, and measured at 51 K.

clearly distinguished in all the samples. The effect of the substrate is more pronounced in the LSMO layers than in Py ones. This result is easily understood taking into account that this electrode is grown onto the substrate. The coercive field of the Py layers is almost independent of the substrate, as expected, and very sensitive to strains at the Py/BSTO.05 interface as appreciated from the H_c vs. t_b plot (Fig. 3(b)). Clearly, it is affected by the lattice relaxation at the barrier as denoted by its variation with the spacer thickness.

The lattice mismatch between LSMO and the two substrates is very different, varying from $\sim 1\%$ for STO to $\sim 8\%$ for MGO. The LSMO accommodates onto MGO by introducing misfit dislocations planes²³ so higher H_c is expected for these layers. The negligible variation of the LSMO coercive field with the spacer thickness for MGO samples denotes that LSMO is more affected by LSMO-substrate interfaces rather than those with the barrier, where the mismatch is much smaller and the film is expected to be strained. On the other hand, LSMO grown on STO is strained at both interfaces due to the close similarity of the crystalline structure of STO and BSTO. Therefore, the coercive field of the strained LSMO appears to be more sensitive to slight variations of the barrier thickness than the LSMO grown on MGO (Fig. 3(c)).

An estimation of the coupling strength was deduced from the measurements of minor loops. This is possible by

measuring minor loop cycles in which the soft Py layer, whose magnetization is in principle parallel aligned with the LSMO magnetization, is forced to flip their magnetization direction in order to reach an antiparallel alignment. Then, the magnetic field is reversed until the magnetization of the soft layer flips again to a parallel state. The shift ΔH of the minor loops hysteresis determines the strength of the magnetic coupling. Following this procedure, the exchange coupling constant J has been calculated for different barrier thicknesses, substrates, and temperatures. A simple free-energy calculation based on the Stoner-Wohlfarth model for single domain layers gives the exchange coupling J in terms of the minor loop coercive fields

$$J = \frac{\Delta H}{2M_{LSMO}},$$

where M_{LSMO} is the saturation magnetization of the LSMO. The model assumes an in plane uniaxial magnetic anisotropy and $J > 0$ ($J < 0$) corresponds to a FM (AF) coupling, respectively.

The thickness dependence of the exchange coupling for both substrates is plotted in Fig. 4 and the error bars correspond to an uncertainty of each coercive field of ± 1 Oe.

The coupling is AF for MGO trilayers. As the barrier thickness increases, J decreases, reaching a minimum value for 2.3 nm and increasing again for thicker barriers. Instead, the coupling in STO trilayers is FM for thin barriers and becomes AF for thicker barriers. The AF coupling strength for $t_b > 2.3$ nm in STO trilayers is comparable to J values measured for MGO ones.

The weak FM coupling observed for the 0.8-STO sample could be attributed to the existence of pinholes, which are more likely as the barrier gets thinner.²⁴ The presence of the AF coupling even for 0.8 nm barrier layers in samples grown on MGO is in agreement with a high surface quality and the absence of pinholes.

The coupling values are one order of magnitude lower than those reported in Fe/MgO/Fe tunnel junctions,²⁴ in which the coupling is governed by spin polarized tunneling. These phenomena is usually explained based on the spin-current Slonczewski's model,¹⁶ which states that the inter-layer exchange coupling results from the torque exerted by rotation of the magnetization from one FM layer relative to

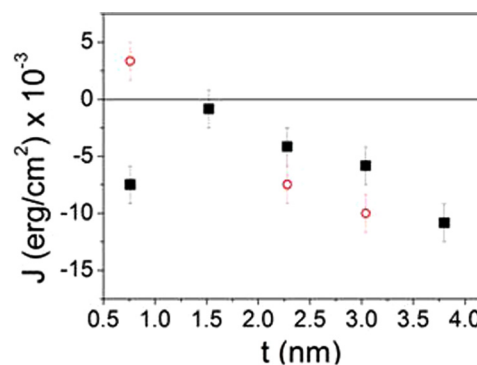


FIG. 4. Exchange coupling J as a function of the barrier thickness t . The values were calculated from minor hysteresis loops measured at 51 K for (red circle) STO and (■) MGO substrates, respectively.

another, and is described in terms of a spin-flip current probability calculated from the stationary wave functions of the free electron Schrödinger equation.²⁵ The model predicts an increasing AF coupling for thinner thicknesses, which agrees with our results for the t_b -MGO series. Discontinuous changes of the potential at the electrode-barrier interface could diminish the spin-polarization factor and are capable of changing the sign of the coupling. The magnitude and sign of J depend on the height of the barrier and the Stoner splitting in the ferromagnets. In contrast to this model and previous reports,^{24–26} no change of sign in the coupling is observed for thicker insulating spacers.

The spin polarization depends on the electron structure of the electrode and also on the electrode-interface character. In the present case, the properties of the spacer comes into play; due to the large dielectric constant values of BST_{0.05},^{27,28} the spacer can partially screen the tunneling electrons between the FM layers and, therefore, reduce the coupling strength. The screening effect together with the charge transfer between LSMO and BST could be responsible for the less pronounced thickness dependence and no change of sign of the coupling. Note that the AF coupling is preserved for barrier thicknesses ranging from 0.8 nm to 3.8 nm; no other AF coupling in junctions with barriers of this range of thicknesses was reported. Most reports²⁴ refer to an orange-peel coupling at larger thicknesses when they have a weak FM coupling. In these samples, our results do not support the hypothesis of a magnetic exchange arisen from interface modulation effects. The orange-peel coupling can be estimated in terms of the wavelength of the roughness oscillations. Based on the Néel model,^{29,30} the orange peel coupling turns out to be no longer than 5×10^{-4} erg/cm³, which is negligible compared to the quantum tunneling coupling; this gives another evidence of the interface quality and low roughness values of our samples. Even though the order of magnitude agrees well with previous reports,³¹ we find a non-monotonic variation of the coupling strength with the spacer thickness for MGO structures. We understand this result as a consequence of the screening effect originated by the high dielectric permittivity of the spacer.

At large barrier thicknesses, Bruno³² proposed a model that explains the AF coupling in terms of the quantum interference due to the (spin-dependent) reflections of Bloch waves at the paramagnet-ferromagnet interfaces. The results for an insulating spacer at $T = 0$ K show that the sign of the coupling at large spacer thicknesses is determined by the Fermi wave vector for majority-spin and minority-spin electrons in a ferromagnet. This model also predicts an increasing coupling with temperature. To further support this model, we analyzed the coupling vs. temperature (Fig. 5). In all cases, the AF coupling increases with temperature, in agreement with Bruno's model. For temperatures higher than 50 K, we observe a plateau, irrespective of the barrier thickness. Assuming a semiconductor barrier, the contribution to the coupling arises from electrons in the valence band close to the Fermi energy, which has a higher probability of being thermally excited as the temperature is increased.³³ At lower temperatures, the slope of the curve is more pronounced and the coupling has a change of sign. These features have already been reported on trilayers of Fe/SC/Fe, where the SC represents different semiconductors spacers.^{34,35} The authors

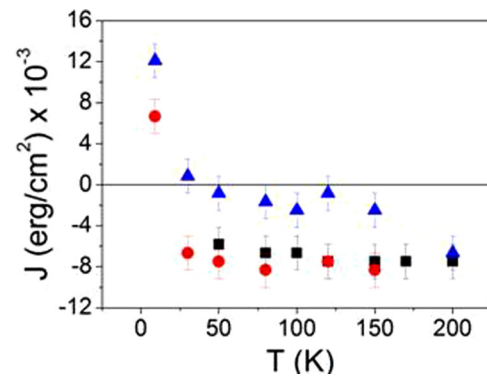


FIG. 5. Interlayer exchange coupling constant, J vs temperature for: (red circle) 0.8-MGO, (blue diamond) 1.5-MGO, and (■) 3.1-MGO, respectively.

propose the existence of a weakly bond electron state, at or near the interfaces that may belong to impurities in the semiconductor material. In our case, the orbital reconstruction at both interfaces could give rise to the formation of these bond states, which in turn leads to an overlap of these states across the interface, with the formation of molecular orbitals.

Previous reports claimed that the oxygen vacancies present at the barrier in Fe/MgO/Fe junctions can fully explain the coupling mechanism. However, theoretical models³¹ predict a coupling strength that decreases with temperature, assuming a barrier that contains impurities or defects. This behavior is opposite to the one shown by our structures and discards the possibility of magnetic coupling dominated by oxygen vacancies at the barrier. Nevertheless, defects or oxygen vacancies could still be present either at the interface or within the insulating spacer.

In summary, we studied the interlayer magnetic coupling in Py/BST_{0.05}/LSMO trilayers for barrier thicknesses of a few unit cells' width, in terms of the temperature and the thickness spacer. An interlayer magnetic coupling produced by a spin-dependent quantum electron tunneling is observed, in which the spin polarization present at the interfaces comes into play. The high dielectric permittivity of the barrier becomes relevant in the coupling, as it screens the tunneling electrons through the FM layers. As a result, the AF interlayer exchange coupling mediated by tunneling currents persists even for thicknesses larger than the already reported values for typical MgO barriers,²⁶ giving the possibility to extend the functionality for larger tunneling barriers. The larger AF coupling observed in samples with thicker barriers is an outstanding result and suggests that further research should be done to explore this phenomenon.

This work was supported by PICTS 1187, 0773, 041, 1047 of FONCYT and PIP112-201101-00482 from CONICET.

¹E. Y. Tsymbal, K. D. Belashchenko, J. P. Velev, S. S. Jaswal, M. van Schilfhaarde, I. I. Oleynik, and D. A. Stewart, *Prog. Mater. Sci.* **52**, 401 (2007).

²P. Zubko, S. Gariglio, M. Gabay, P. Ghosez, and J.-M. Triscone, *Annu. Rev. Condens. Matter Phys.* **2**, 141 (2011).

³J. J.-H. Park, E. Vescovo, H.-J. Kim, C. Kwon, R. Ramesh, and T. Venkatesan, *Nature* **392**, 794–796 (1998).

⁴M. Bibes, J. E. Villegas, and A. Barthélémy, *Adv. Phys.* **60**, 5 (2011).

⁵W. Feng and W. Che, *IEEE Microwave Wireless Compon. Lett.* **22**, 562 (2012).

- ⁶P. M. Suherman, H. T. Su, T. J. Jackson, F. Huang, and M. J. Lancaster, *Ferroelectrics* **367**, 170 (2008).
- ⁷F. Tsui, M. C. Smoak, T. K. Nath, and C. B. Eom, *Appl. Phys. Lett.* **76**, 2421 (2000).
- ⁸R. A. Chacalov, Z. G. Ivanov, Yu. A. Boikov, P. Larsson, E. Carlsson, S. Gevorgian, and T. Claeson, *Physica C* **308**, 279 (1998).
- ⁹V. Garcia, M. Bibes, and A. Barthelemy, *C. R. Phys.* **16**, 168 (2015).
- ¹⁰F. Michelini, L. Ressler, J. Degauque, P. Baulès, A. R. Fert, J. P. Peyrade, and J. F. Bobo, *J. Appl. Phys.* **92**, 7337 (2002).
- ¹¹V. Garcia, M. Bibes, A. Barthélémy, M. Bowen, E. Jacquet, J.-P. Contour, and A. Fert, *Phys. Rev. B* **69**, 052403 (2004).
- ¹²F. Y. Bruno, J. Garcia-Barriocanal, M. Varela, N. M. Nemes, P. Thakur, J. C. Cezar, N. B. Brookes, A. Rivera-Calzada, M. Garcia-Hernandez, C. Leon, S. Okamoto, S. J. Pennycook, and J. Santamaria, *Phys. Rev. Lett.* **106**, 147205 (2011).
- ¹³H. Yamada, Y. Ogawa, Y. Ishii, H. Sato, M. Kawasaki, H. Akoh, and Y. Tokura, *Science* **305**, 646 (2004).
- ¹⁴J. C. Rojas Sánchez, B. Nelson-Cheeseman, M. Granada, E. Arenholz, and L. B. Steren, *Phys. Rev. B* **85**, 094427 (2012).
- ¹⁵M. Y. Zhuravlev, A. Vedyayev, and E. Tsymlal, *J. Phys.: Condens. Matter* **22**, 352203 (2010).
- ¹⁶J. C. Slonczewski, *Phys. Rev. B* **39**, 6995 (1989).
- ¹⁷M. Sirena, E. Kaul, M. B. Pedreros, C. A. Rodriguez, J. Guimpel, and L. B. Steren, *J. Appl. Phys.* **109**, 123920 (2011).
- ¹⁸J. C. A. Huang, T. E. Wang, C. C. Yu, Y. M. Hu, P. B. Lee, and M. S. Yang, *J. Cryst. Growth* **171**, 442 (1997).
- ¹⁹A. Ruotolo, A. Oropallo, F. Miletto Granozio, G. P. Pepe, P. Perna, and U. Scotti di Uccio, *Appl. Phys. Lett.* **88**, 252504 (2006).
- ²⁰M. Ohtake, T. Tanaka, K. Matsubara, F. Kirino, and M. Futamoto, *J. Phys.: Conf. Ser.* **303**, 012015 (2011).
- ²¹L. F. Yin, D. H. Wei, N. Lei, L. H. Zhou, C. S. Tian, G. S. Dong, X. F. Jin, L. P. Guo, Q. J. Jia, and R. Q. Wu, *Phys. Rev. Lett.* **97**, 067203 (2006).
- ²²L. B. Steren, M. Sirena, and J. Guimpel, *J. Appl. Phys.* **87**, 6755 (2000).
- ²³L. B. Steren, M. Sirena, and J. Guimpel, *J. Magn. Magn. Mater.* **211**, 28 (2000).
- ²⁴J. Faure-Vincent, C. Tiusan, C. Bellouard, E. Popova, M. Hehn, F. Montaigne, A. Schuhl, and E. Snoeck, *J. Appl. Phys.* **93**, 7519 (2003).
- ²⁵J. Faure-Vincent, C. Tiusan, C. Bellouard, E. Popova, M. Hehn, F. Montaigne, and A. Schuhl, *Phys. Rev. Lett.* **89**, 107206 (2002).
- ²⁶T. Katayama, S. Yuasa, J. Velev, M. Ye. Zhuravlev, S. S. Jaswal, and E. Y. Tsymlal, *Appl. Phys. Lett.* **89**, 112503 (2006).
- ²⁷Z. Zhao, X. Wang, K. Choi, C. Lugo, and A. T. Hunt, *IEEE Trans. Microwave Theory Tech.* **55**, 430 (2007).
- ²⁸V. Craciun and R. K. Singh, *Appl. Phys. Lett.* **76**, 1932 (2000).
- ²⁹L. Néel, *Comptes Rendus Acad. Sci.* **255**, 1545 (1962).
- ³⁰L. Néel, *Comptes Rendus Acad. Sci.* **255**, 1676 (1962).
- ³¹M. Ye. Zhuravlev, E. Y. Tsymlal, and A. V. Vedyayev, *Phys. Rev. Lett.* **94**, 026806 (2005).
- ³²P. Bruno, *Phys. Rev. B* **52**, 411 (1995).
- ³³J. Varalda, J. Milano, A. J. A. de Oliveira, E. M. Kakuno, I. Mazzaro, D. H. Mosca, L. B. Steren, M. Eddrief, M. Marangolo, D. Demaille, and V. H. Etgens, *J. Phys. C: Condens. Matter* **18**, 9105 (2006).
- ³⁴M. Hunziker and M. Landolt, *Phys. Rev. Lett.* **84**, 4713 (2000).
- ³⁵P. Walser, M. Hunziker, T. Speck, and M. Landolt, *Phys. Rev. B* **60**, 4082 (1999).